Petroleum xxx (xxxx) xxx–xxx

Contents lists available at ScienceDirect

Petroleum

journal homepage: http://www.keaipublishing.com/en/journals/petroleum

Fault reactivation potential and associated permeability evolution under changing injection conditions

Dorcas S. Eyinla[a,b,c,*], Michael A. Oladunjoye[a], Quan Gan[c], Abel I. Olayinka[a]

[a] Department of Geology, Pan African University, Life and Earth Sciences Institute (PAULESI), University of Ibadan, Ibadan, Nigeria
[b] Department of Earth Sciences, Adekunle Ajasin University, Akungba Akoko, Nigeria
[c] Department of Petroleum Geology and Geology, School of Geosciences, University of Aberdeen, Aberdeen, Scotland, UK

ARTICLE INFO

Keywords:
Fluid pressure diffusivity
Shear deformation
Pressure elevation
Injector location
Slip magnitude

ABSTRACT

Understanding the hydraulic and frictional sensitivity of fault to different injection conditions is one of the efficient ways to provide useful implications for fault reactivation potential. Numerical simulations of fractured reservoir have provided information on how fault behaviour varies under changing hydromechanical properties and injection conditions. A coupled hydro-mechanical model which can represent the elastoplastic behaviour of a fault was employed to predict and quantify the effects of varying injection positions and injection rates on permeability response and potential of fault reactivation under isothermal injection. We examine the sensitivity of seismic event magnitude and timing to variations in both pressure perturbation and stress as injection location changes. We generate results for two scenarios: one with changing injection position but with uniform injection rate, and another scenario with increasing injection rate at the same injection position. We observed that the potential of fault reactivation is affected by the hydraulic diffusivity potential of the fluid pressure, and this mechanism is mediated by a function of the injector position and injection rate. As the velocity of fluid transmission increases, increasing fluid pressure impact pore pressure elevation and reduced effective stress. However, an injector position where there is low diffusivity causes low pore pressure build-up rate, incapable of inducing shear failure, and thus, permeability enhancement is retarded in this case. Accordingly, the injection rate variation influences the rate of pore pressure build-up, the timing and magnitude of induced seismic events. This is also reflected in the permeability evolution as a response to the variations in the magnitude of fault openings and cracks. This changing injection conditions however influences the timing required to reach the critical peak friction point as pore pressure build-up rate and sensitivity to loading response change. Hence, with changing position and rate of injection, the evolution of fault permeability appears to be intrinsically controlled by a condition which favours elastoplastic deformation and fracture failure, with slip distance increasing with high injection rates.

1. Introduction

Fracture systems in rock mass are usually complex, and these increase the uncertainty in their quantification and analysis with numerical simulation. With increasing rate of Enhanced Geothermal Systems and fracking, the complexity of fractures influences the variations in the hydraulic response, and this has been reported to have a significant interference with the injection process [1–3]. Therefore, to ensure maximum production rate with minimized production cost, one of the key factors to consider in hydraulic fracturing is the choice of the fit working parameters which include injection fluid type, injection flow rate and frequency, and number of fracturing phases [4–6]. Another important factor is the choice of injector location, which would determine the proper distribution of pressure and stress for adequate fracture response and proper well management [5,7]. So, situating the injection well in the right location where maximum production can be achieved is one of the major decision engineers must make before embarking on the recovery process of subsurface energy.

Generally, fracture stimulation has been identified to increase the production rate and has been credited with adding to the initial quantity of reserves. According to Montgomery and Smith [8] report, 9 billion barrels of oil and above 700 Tscf (Trillion of standard cubic feet) of gas had been added to US reserves since 1949, which possibly would have been unprofitable to develop. Nevertheless, the negative effect of

Peer review under responsibility of Southwest Petroleum University.
* Corresponding author. Department of Geology, Pan African University, Life and Earth Sciences Institute (PAULESI), University of Ibadan, Ibadan, Nigeria.
E-mail address: dorcas.eyinla@aaua.edu.ng (D.S. Eyinla).

https://doi.org/10.1016/j.petlm.2020.09.006
Received 12 January 2020; Received in revised form 15 June 2020; Accepted 14 September 2020

fractures is that it can provide paths through which injected water/steam can bypass the matrix pores causing a slowdown or abrupt termination of hydrocarbon production [9]. In both cases, an optimized field development plan and enhanced hydrocarbon recovery can only be achieved by locating subsurface fractured zones, knowing their geomechanical properties and geometry, and predicting the most appropriate location to place the injection well.

Under normal hydraulic stimulation, shear stimulation and slip have been recognized as dominant mechanism for promoting permeability enhancement, except in the situation involving thermally induced tensile fracturing [10,11]. Expectedly, pressure build-up caused by fluid injection will decrease the response of effective stress, which may affect fault stability. The poroelastic effect caused by pressure build-up varies as the injection condition changes. Therefore, when injecting into a low-permeable fault, pressure would be induced between the injection well and the fault, however, the velocity of fluid transmission would have considerate impact on the amount of resulting pressure build-up. This fluid velocity is highly dependent on the injection rate and the position around the fault where the injection takes place [7].

Relatively, reports have shown that the slip behaviour of faults during injection is attributed to several factors including the frictional sliding resistance of the fault and joints, the direction and amount of stress field, and pressure distribution pattern [12]. The instability of a fault is dependent on several factors including the fault dip angle, which determines the angle between the fault plane and the direction of principal stress orientation [13]. As reports suggested, higher fault angle creates higher pressure build-up, consequently, more slip and shear failure. Nonetheless, the key features in hydraulic fracturing include pressure breakdown and morphology of the induced fractures. However, these are highly dependent on both the fracturing fluid type and the condition of applied stress [14]. The work of Gan and Elsworth [15] explored various stimulation strategies to examine the impact of stimulation direction relative to the orientation of a pre-existing fracture network, with emphasis on the magnitude and lifespan of thermal recovery rates. In this situation, the variation in stress distribution was considered as a function of the injector position and the pressure build-up as injection rate increases. Notably, higher injection rate does not only promote faster pressure build-up, it also influences the timing required to reach the critical peak friction value [16]. An intrinsic correlation exists between elastic strength and fracture pressure, such that the pore pressure and fracture pressure decrease when the elastic properties of materials is higher [17]. This implies that with an increasing geomechanical strength of geological material, a lesser amount of pressure is required to initiate hydraulic fractures into them. However, the hydraulic diffusivity of the fluid pressure also places a highly significant influence on the resulting pore pressure evolution, which partly determines the fault slip tendency [18]. A situation where effective stress evolves corresponding to pore pressure elevation, depending on the initial stress regime, the Mohr's circle will expand or shrink while shifting towards hydromechanical failure [19,20]. Clearly, hydraulic diffusivity controls the fluid pressure and thus influences the response of the effective normal stress during shear failure [21]. This is a fundamental part of any injection process when fracture slip is intended because the diffusivity controls the amount of fluid overpressure that can be maintained on a fault, and from all indications, the evolution of fluid pressure controls the mechanism of failure [21,22].

With hydromechanical stimulation, shear failure has been recognized as a dominant mechanism which promotes permeability enhancement, with the contributing influence of thermally induced tensile fracturing, like thermal stress when injection temperature varied from the reservoir temperature [16,23]. To achieve a successful simulation of an unconventional reservoir model, the specific properties of both host rock and natural fractures must be established. These properties include the compression and tensile strength of the materials, the initial porosity and permeability, the modulus of strength [24]. These properties influence the hydromechanical response of fault when subjected to an amount of stress during injection, consequently, the resulting fracture permeability is dependent on several factors which include the geomechanical properties of the matrix rock and the discontinuities, and the prevailing injection conditions.

Faults constitutive properties reproduce some distinctive fault slip phenomena which include slip instabilities when stresses rise above critical stress level, a more important part is the recovery of fault strength following slip instability due to shear slip [25]. The phenomenon of how faults regain strength during earthquakes is crucial for our understanding of fault healing and fracture closure during numerical simulation of fault injection. While several factors have been presented as a possible cause, the most important factor which could play a role in hydromechanical interaction is the frictional strengthening [26].

An interplay between permeability evolution and fault strength enables a better understanding of fault behaviour as fluid pressure is induced. Therefore, fault permeability behaviour and mechanical failures could be investigated through response to localized pressurization influenced by well placement and rate of injection. The aim of this study is therefore to first investigate how the position of injector along the fault plane influences fault permeability evolution and the reactivation potential of a fault with uniform injection rate. We then further consider how increasing injection rate promotes fault reactivation tendency and the effect on permeability evolution.

2. Theory and methodology

The mechanical and hydraulic properties of fault may be isotropic or anisotropic depending on the architecture of the fault [23], however, permeability change is often linked to the nonlinear normal stress and the permeability function while considering the plastic strain dilation in the model [27]. Our model assumed an anisotropic constitutive elastoplastic model developed in FLAC3D as an ubiquitously fractured media [23,27,28].

2.1. Hydraulic diffusivity

Considering an ideal case where fluid is injected into an elastoplastic medium at a specific point and with a constant injection rate. The ratio of total stress change to change in pore ($\Delta\sigma/\Delta p$) can be expressed in terms of the material's Poisson's ratio (ν), the Biot's coefficient (α), and the Boltzmann variable $\xi = ((x_k x_k)/c_d/t)^{\frac{1}{2}}$. The Boltzmann variable is a function which depends on the hydraulic diffusivity and time of injection [19,20,29] with the following relationship;

$$\frac{\Delta\sigma_{ij(x,t)}}{\Delta p(x,\,t)} = \frac{\alpha(1-2\nu)\left\{\delta_{ij}\left[erfc\left(\left(\frac{1}{2}\right)\xi\right) - \left(\frac{2}{\xi^2}\right)g(\xi)\right] + \left(\frac{x_i x_j}{r^2}\right)\left[erfc\left(\left(\frac{1}{2}\right)\xi\right) + \left(\frac{6}{\xi^2}\right)g(\xi)\right]\right\}}{2(1-\nu)erfc\left(\left(\frac{1}{2}\right)\xi\right)}$$

where, $g(\xi) = \frac{1}{2\sqrt{\pi}}\int_0^{\xi} s^2\exp\left(-\frac{1}{4}s^2\right)ds = erf\left(\frac{1}{2}\xi\right) - \frac{\xi}{\sqrt{\pi}}\exp\left(-\frac{1}{4}\xi^2\right)$.

The hydraulic diffusivity controls the rate of fluid pressure circulation, and thus, influences the resulting effective normal stress during shear deformation [21]. The difference in the hydraulic behaviour of fault with the same properties could be linked to the contrast in hydraulic diffusivity in the fault zone elements [30].

2.2. Fault permeability and aperture evolution

Fault initial permeability is assumed to be higher than the permeability of the host rock (matrix) as shown in Table 1. To satisfy the requirement for representing coupled elastoplastic behaviour of fault, the permeability of fractures in the fault zone has been modelled using Warren and Root [31] approach as it connects the fracture aperture and

Table 1
Data used in the simulation.

Parameter (unit)	Magnitude
Bulk modulus (GPa)	15 (host rock), 1.5 (fault)
Poisson's ratio	0.22
Fluid compressibility ($\mathbf{MPa}^{-1}$)	4.2×10^{-4}
Biot's coefficient (α)	1
Matrix porosity ($\varnothing_{\mathbf{m}}$)	0.01
Matrix permeability ($\mathbf{m}^2$)	1.0×10^{-16}
Thermal expansion coefficient of solid ($\mathbf{K}^{-1}$)	12×10^{-6}
Initial reservoir pore pressure (MPa)	13.8
Minimum principal stress (MPa) —x direction	27.3
Maximum principal stress (MPa) —z direction	45.5
Fracture aperture initial (mm)	1
Fracture spacing (m)	0.5
Initial joint shear stiffness (GPa/m)	50
Initial joint normal stiffness (GPa/m)	0.5
Thermal diffusivity of intact porous rock ($\mathbf{m}^2$/s)	1.1×10^{-6}
Fluid density ($\mathbf{kg}/\mathbf{m}^3$)	1000
Heat capacity of fluid (J/kg K)	4.26×10^5
Initial reservoir temperature (°C)	200
Joint friction angle, dilation angle (°)	28
Matrix friction angle (°)	45
Rock density ($\mathbf{kg}/\mathbf{m}^3$)	2700
Fracture permeability, m^2	1.0×10^{-14}
Dilation angle (°)	0 (host rock), 5 (fault)
Cohesion (MPa)	3 (host rock), 0 (fault)
Porosity	0.01 (host rock), 0.3 (fault)

fracture spacing thus;

$$k = \frac{b^3}{12s} \tag{1}$$

Where k is the fault permeability, b is the fracture aperture, and s is the fracture spacing.

Fig. 1a represents a stress-dependent aperture evolution, where the effect of stress state has a direct impact on changing the fracture aperture. This type of stress-dependent permeability model results in changing the compliance tensor in the simulation loop [15,32,33]. The figure clearly illustrates the constitutive relation of fracture aperture evolution with stress state as applicable to our model. The curve extending to the right represents the feature under normal closure and shear dilation. In this case, the moment the fluid pressure approaches the critical magnitude point (P_{f0}) where effective normal stress becomes zero, a geometrical stiffness (K_{gf}) is adopted to estimate the induced normal opening displacement when the two walls are subjected to tension.

The fault normal opening displacement is assumed linear, and the fluid pressure increment is based on this relationship, $P_f - P_{f0}$ [15]. From this relationship, the equation for the fracture opening displacement (b_{open}) is formulated by Gan and Elsworth [15] as,

$$b_{\text{open}} = \frac{P_f - P_{f0}}{K_{gf}} = \frac{P_f - P_{f0}}{10K_s^{\text{rock}}} = \frac{(P_f - P_{f0})}{10 \times \frac{7\pi}{24}\frac{G}{r}} \tag{2}$$

To fully represent the relationship of stress-dependent aperture change (including normal closure) with shear dilation, and fracture opening, the fracture aperture is given as;

$$b = b_{ini} - \frac{9b_{ini}\sigma_n'}{\sigma_{nc} + 10\sigma_n'} + \frac{\tau - \tau_{sc}}{K_s}\tan\varphi_d + \frac{(P_f - P_{f0})}{10 \times \frac{7\pi}{24}\frac{G}{r}} \tag{3}$$

Where G is the shear modulus of the intact rock, b_{ini} is the initial aperture of the fracture, b_{normal} is the reduction of aperture due to the normal closure, K_s^{rock} is the geometrical stiffness, σ_n' is the effective normal stress of the fracture, σ_{nc} is the critical normal stress, τ_{sc} is the critical shear stress at the point of failure.

Our model demonstrates the sensitivity of fault permeability to hydromechanical behaviour, and changes in normal stress or volumetric strain will influence a change in fault normal displacement, and as a result, permeability enhancement is expected at the onset of slip. So, for a fractured medium adopted in this study, models for

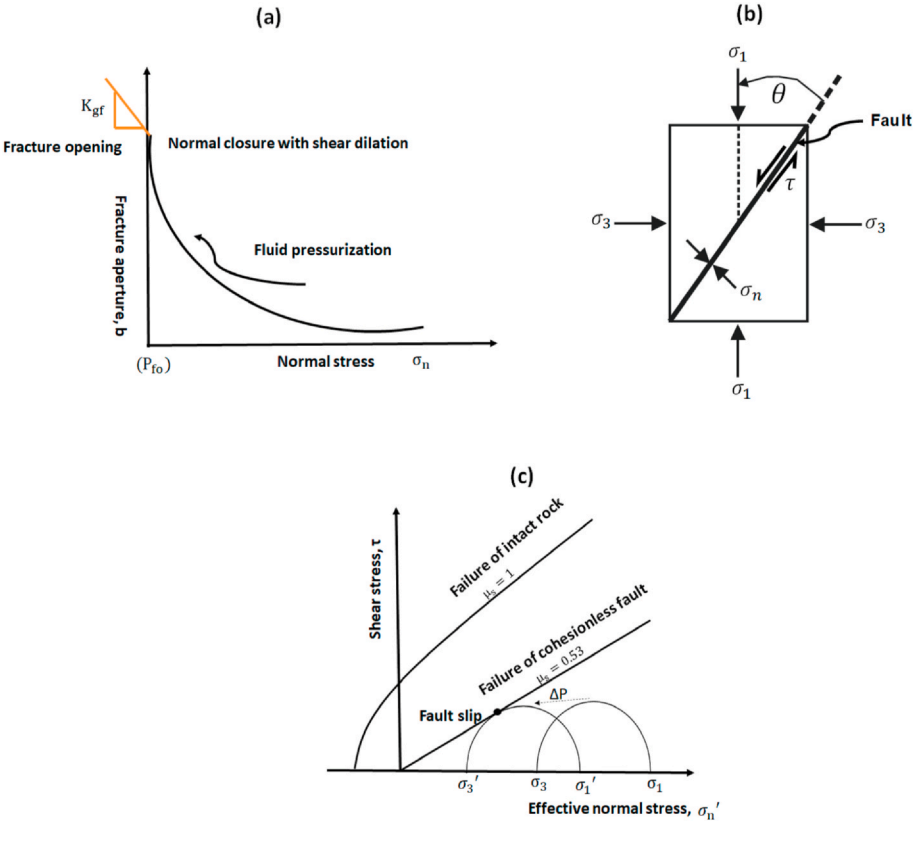

Fig. 1. (a) Evolution of Fracture aperture under different normal stress state (modified from Gan and Elsworth [15]), (b)Resolution of normal and stresses along a fault plane with a given orientation from the remote principal stresses (modified from Cappa and Rutqvist [23], (c) Shear stress against effective normal stress showing slip failure mechanism by fluid pressurization (modified from Gan and Elsworth, [34].

permeability change as governed by the input involves the growth in the fracture aperture, which may be defined by an empirical function of nonlinear fracture stiffness and applied effective stress according to Rutqvist et al. [45].

2.3. Failure criteria

During fluid injection, reactivation of pre-existing fault is likely to occur depending on the maximum sustainable pressure limit and principal stress resolution [20]. Fig. 1b shows the dynamics of stress resolution on the fault plane, a configuration which allows fault re-activation through shear slip when the frictional limit of the fault is exceeded. The Mohr's circle will expand or shrink (Fig. 1c), technically, whenever shear displacement occurs, it is usually accompanied with a shear dilation [35]. This behaviour promotes permeability enhancement at slip. For our model, the simulation is designed to yield permeability increase during slip, because of the dilation angle of the fault [16,18]. Hence, using the Gan and Elsworth [34] approach, the magnitude of normal stress and shear stress acting on a fault plane is modified thus;

$$\sigma_{neff} = \frac{\sigma_3 + \sigma_1}{2} + \frac{\sigma_3 - \sigma_1}{2}\cos 2\theta + \tau_{xz}\sin 2\theta - P \tag{4}$$

$$\tau = \frac{\sigma_1 - \sigma_3}{2}\sin 2\theta + \tau_{xz}\cos 2\theta \tag{5}$$

Where σ_{neff} represents the effective stress, P is pore fluid pressure, σ_1 is the maximum principal stress, σ_3 is the minimum principal stress and the angle between the fault plane and the maximum principal stress is given as θ. However, considering our simulation output data, these relationships interpret to the following:

$$\sigma_{neff} = \frac{S_{xx} + S_{zz}}{2} + \frac{S_{xx} - S_{zz}}{2}\cos 2\theta + S_{xz}\sin 2\theta - P \tag{6}$$

$$\tau = \frac{S_{zz} - S_{xx}}{2}\sin 2\theta + S_{xz}\cos 2\theta \tag{7}$$

Where S_{zz} is the maximum principal stress (stress in the vertical direction), S_{xx} is the minimum principal stress (stress in the horizontal direction) and S_{xz} is the shear component of the stress.

2.4. Shear slip theory

Analytical techniques for studying fault reactivation are conducted using the magnitude and orientation of principal stress with respect to existing fault planes and fluid pressure along the fault plane [13,36]. Mechanical shearing often produces extreme changes in the texture of fault gouge materials whenever slip occurs [37].

A classical approach to isotropic Coulomb friction model allows all contact analysis capabilities. This approach assumes that there is no relative motion if the equivalent frictional stress expressed as $\tau_{eq} = \sqrt{\tau_1^2 + \tau_2^2}$ is lower than the critical stress, τ_{crit}, where τ_1 is the critical shear stress surface in the horizontal direction and τ_2 is the critical shear stress surface in the vertical direction. However, the critical stress is proportional to the contact pressure p, such that the established relationship is given as $\tau_{crit} = \mu p$. Here, μ is known as the friction coefficient which can be defined in terms of the contact pressure p, the slip rate, and other factors. Notably, if the equivalent stress is at the state of critical stress, that is, $\tau_{eq} = \tau_{crit}$, then it is most likely that a slip can occur [38].

Slip tendency is regarded as the likelihood of a fault plane to slip during injection when subjected to a certain level of stress. This is highly dependent on the frictional resistance of the joints and the ratio of shear to normal stress acting on that surface.

In hydromechanical interaction, a commonly used relationship which describes the fault slip along a plane is the Mohr-Coulomb shear failure criterion [20].

According to Ref. [23], this relationship has been simplified as:

$$\tau = c + \mu_s \sigma_n' \tag{8}$$

And according to the Terzaghi [39], effective stress law has been defined as:

$$\sigma_n' = \sigma_n - P \tag{9}$$

Where τ is the critical shear stress for slip occurrence, c as the cohesion, μ_s is the static friction coefficient, σ_n' is the effective normal stress, σ_n is the total normal stress and P is fluid pressure.

Also, the static friction coefficient, μ_s, has been defined by Biot [40] and Byerlee [41] as,

$$\mu_s = \tan\varphi \tag{10}$$

Where φ is the friction angle.

For this study, we adopted the Coulomb stress ratio, η, which defines the ratio of shear stress to effective stress (Fig. 1b) as:

$$\eta = \tau/\sigma_{neff} \tag{11}$$

Evolution of Coulomb stress ratio for each injection scenario would afford the opportunity to monitor frictional resistance of the fault and allow a more detailed study of the shear evolution throughout the injection process. This ratio has also been adopted in determining the slip tendency and the timing required to reach the critical peak friction value during pore pressure elevation [16].

According to Jaeger and Cook [42]; Cappa and Rutqvist [23] and Gan and Elsworth [34]), a slip can occur on the surface when the Coulomb stress ratio is greater than or equal to the frictional resistance to sliding. However, our study has adopted an internal fault friction angle of 28°, consequently, the coefficient of friction, μ_s would be 0.53 (tan 28°) · Therefore, for a slip to occur, the critical peak friction value must be greater than or equal to 0.53 (That is, $\eta = \tau/\sigma_n \geq \mu_s$).

2.5. Model setup

Fig. 2 shows the reservoir geometry for this study with the critically stressed normal fault of length 424 m and width 2 m, which was inclined at angle 45° to the principal stresses. The fault is embedded within a reservoir model geometry with spatial dimension 600 m × 15 m x 600 m. The injection well is assumed in three scenarios: at the top of the fault, at the centre of the fault and at the bottom (Fig. 3a, b and c). The response of fault to each injection position was examined with a constant injection rate of 0.5 kg/s, while the minimum principal stress acting on x-direction is 27.3 MPa and the maximum principal stress is set at 45.5 MPa (z-direction). We also investigate the effect of increasing injection rate on permeability enhancement and slip tendency.

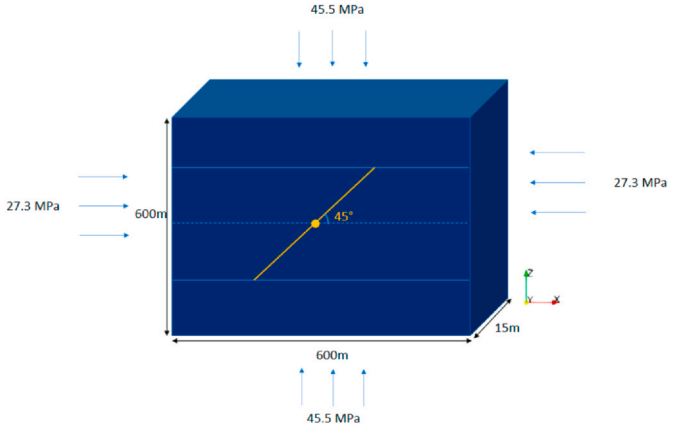

Fig. 2. Model geometry showing the position of the fault in a confined reservoir subjected to stresses on all sides.

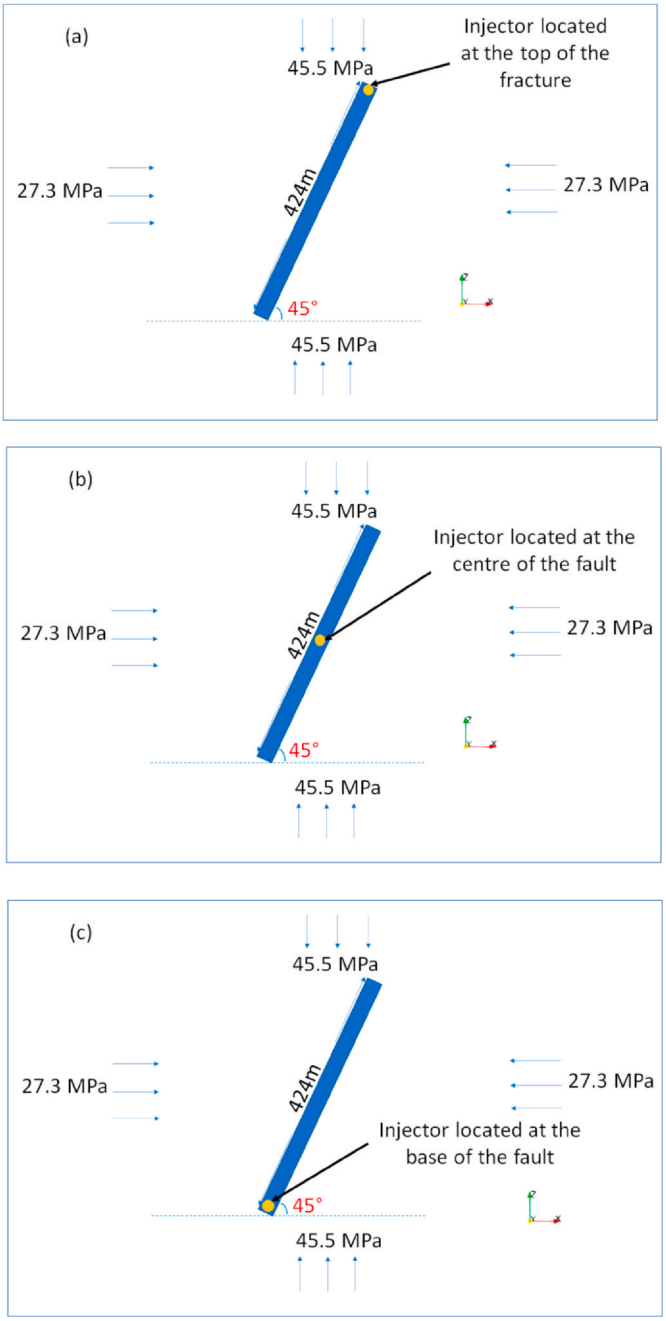

Fig. 3. Schematic representation of fault injection with (a) top injection (b) mid injection (c) bottom injection.

Table 2
Injection conditions for this study.

SCENARIOS	INJECTOR POSITION	INJECTION RATE (KG/S)
Case A	Top injection	0.5
	Mid injection	0.5
	Bottom injection	0.5
Case B	Mid injection	0.10
	Mid injection	0.20
	Mid injection	0.25
	Mid injection	0.28
	Mid injection	0.30

Data in Table 1 present the assumed properties for the matrix and fault zone used for the numerical simulation. The injection was carried out in isothermal condition using the continuum simulator TOUGHREACT-FLAC3D developed by Taron et al. [43]with coupled hydro-mechanical process, which links the TOUGHREACT multiphase flow with the FLAC3D geomechanical simulator [44]. The elastoplastic behaviour of the fault zones represents a combination of solid elements and ubiquitous joints occurring as weak planes [23] and the fault assumes a Mohr-Coulomb slip behaviour such that there is shear failure when the shear strength is exceeded [16,34,45]. Table 2 shows the injection scenarios which examines the effects of injection position and injection rate.

3. Results and discussion

The simulation of hydraulic fractures in this model involves investigation of fault sensitivity to changing injection position, and how a chosen injection rate influences fault permeability evolution and possible reactivation. We compare results for three distinct injection positions, as well as increasing injection rates at the same injection position (middle of the fault). The results for various numerical simulations scenarios as listed in Table 2 are analysed and interpreted. Our results illustrate how fault permeability evolution have a first order control on the growth of aseismic slip relative to the diffusivity potential of fluid pressure.

3.1. Effect of injection position

The evolving permeability from various injection location revealed dissimilar response, although the top and middle injection have closely related permeability evolution pattern (Fig. 4a). Injecting at the base of the fault yielded no significant enhancement of permeability evolution when compared with the other two locations, as the pressure elevation in the bottom condition could not be sufficient to trigger shear slip failure. Seemingly, fault slip activities promote the significant permeability enhancement observed in most injection program, as fault failure is the driving force which induces fault opening [16,18]. Our study adopts the Coulomb failure theory, where shear slip along a fault can only occur when the shear stress to effective normal stress ratio exceeds the frictional coefficient on the fault plane [18,34,45,46], consequently, the slip potential of fault in each injection model controls the non-uniformity in permeability evolution observed. Structurally, fault opens during fluid injection, and the implication of this is that permeability variation is in close relation to the evolution of fluid pressure [30,35,47]. With the injector positioned at the top and fault centre, there is a gradual permeability increase during unloading, meanwhile, the most energetic event and complex interplay occur during the phase of hydraulic unloading [48]. The increase in fault permeability during aseismic slip period represents the largest cumulative permeability increase during injection, from the magnitude of 10^{-15} to 10^{-12} in both cases (top and mid injections). This permeability enhancement is mostly because of the opening of faults during sliding [47]. As observed, the fluid pressure evolution in these two scenarios were distinctly elevated throughout the injection period (Fig. 4c).

The slight permeability rise noticed when injecting from the base of the fault is possibly reflecting the mechanism of less compaction during injection. This position presents no significant stress change (Fig. 4d), and shear stress accumulation is almost uniform with no shear failure (Fig. 4e). Expectedly, when a sufficient part of the fault is already pressurized and weakened, a corresponding fault slip accelerates. However, with injector at the base of the fault, lateral diffusion of fluid pressure from this position is not sufficient to pressurize a substantial part of the fault to shear failure. A higher fluid pressure would diffuse faster and more effectively to the targeted zone when the injection source originates from the upper part of the fault. This explains why

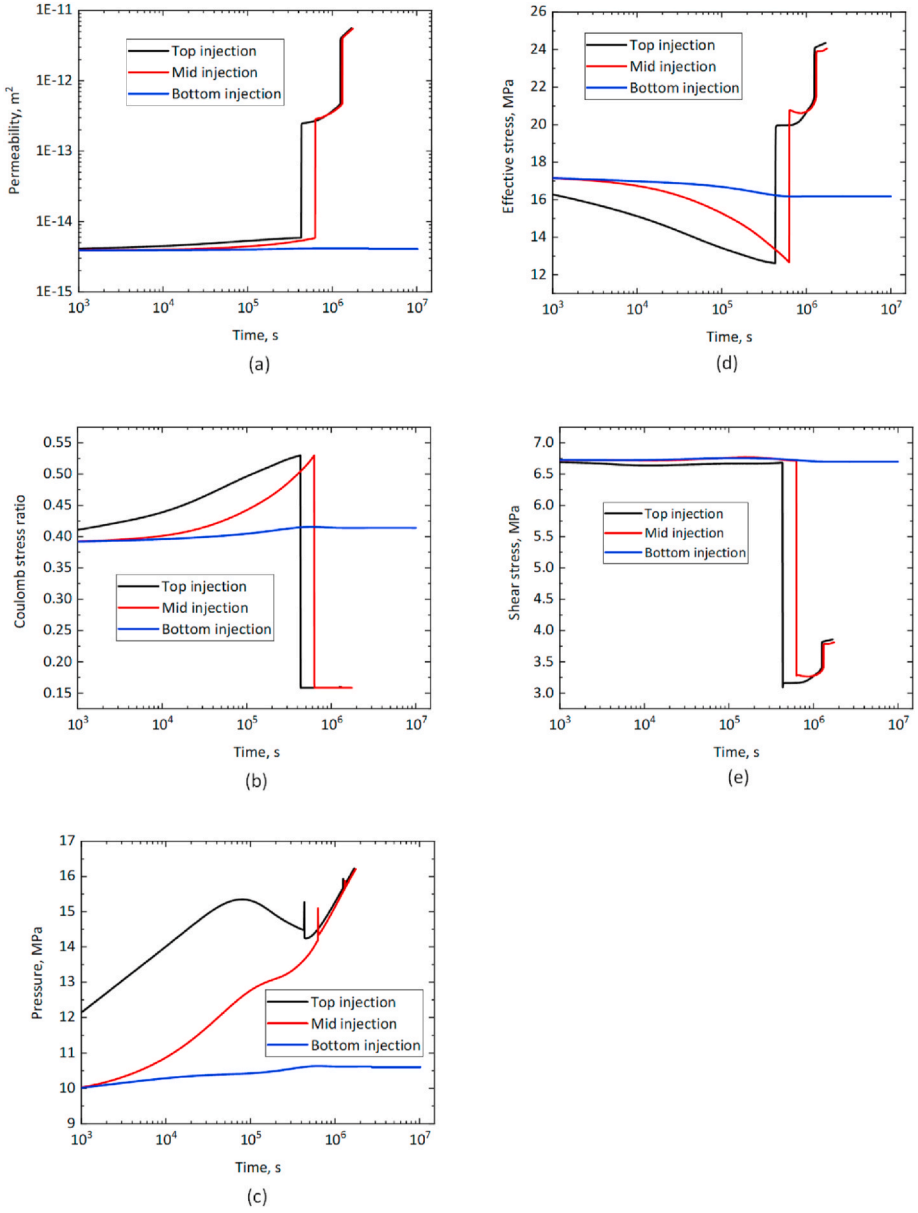

Fig. 4. (a) Evolution of fault permeability at different injector positions (b) Evolution of Coulomb stress ratio showing variation in slip tendency with changing injection position (c) Evolution of pore pressure at various injection positions (d) Evolution effective stress with as injector position changes (e) Evolution of shear stress at various injection positions [47]. Thus, permeability increases as the pore pressure increases [49] and effective stress increases during hydraulic loading.

pressure and permeability gradients decrease as injector position decreases with depth, with top injection having the highest pore pressure and permeability followed by mid injection and then bottom injection. Observations therefore showed that increasing fluid pressure diffusion instigates fault opening and shear slip which promotes permeability enhancement [18]. Which means variation in fault permeability is intrinsically controlled by the evolution of fluid pressure and effective stress.

Notably, for top injection, there is a decreasing pressure before fracture slip after an earlier continuous rise from the commencement of injection. Pressure rises to a point where there is a need to re-equilibrate, to ensure fault stability. Thus, there is a gradual pressure diffusion from the fault into the matrix surrounding [50] which is recorded on the pressure evolution profile as a declination in pressure. However, after a steady pressure state is reached, shear slip occurred resulting in undrained pore pressure. This implies that changes in permeability causes pore pressure redistribution [50], because the sudden enhancement of pore pressure is due to the fault opening, creating more permeable channel for increasing pressure build-up. The steep pressure surge corresponds to the timing of shear failure in both top and mid injection (Fig. 4b and c). Meanwhile, with dilation and increased volumetric strain, there is diffusion of the accumulated pore pressure which helps to maintain continuity of pore pressure level and fluid flux across the fault [16,51,52].

Evolution of Coulomb stress is dependent on the shear accumulation potential and frictional resistance of the fault. Thus, frictional resistance increases as the diffusion rate decreases during injection, and this reflects the increasing of slip tendency when injecting at the top than the mid and base of the fault because of higher hydraulic diffusivity at the top (Fig. 4c).

The evolution of fault hydraulic features enables a distinct behaviour of slip growth during fluid injection as pore pressure is build-up at both locations and poroelastic effect influences the observed permeability evolution [19,20,53,54]. However, our model results with bottom injection indicated a low pressure build up (Fig. 4c), unlike the continuous pressure build-up along the fault plane shown in the other

two injector locations. The variation in this hydraulic response is a function of the impact of the lateral diffusivity of fluid pressure whose impact is highest when the pressurized zone is relatively above the targeted fault plane, as in the case of top injection (Fig. 4c). Accordingly, aseismic slip grows beyond the pressurized zone, and the perturbation of fluid pressure produces lateral diffusion along the fault from the injector point [18]. Consequently, lateral diffusion of fluid pressure did not trigger sufficient pore pressure elevation and injection-induced aseismic slip with the injector at the base of the fault. The background stress is very low, and the frictional weakening is not able to release shear slip. The main effect of fluid pressure diffusion is to release pore pressure growth which can create instability of the fault plane while elevating the effective stress that is sensitive to loading response. However, with a possible upward movement of the injection fluid while injecting at the base of the fault, the velocity and diffusivity of the fluid pressure is considerably reduced, consequently, pressure build-up in the fault is consistently low and ineffective, therefore, the fault remains stiff and insensitive to unloading and loading. Perhaps, this suggests that the fluid pressures acting on them must be lower, and if these pressures do not gain the required velocity of fluid migration to the overlying fault, the much less elevated fluid pressures would be inadequate to cause pore pressure rise, to create fault reactivation.

Notably, elevated fluid pressure can cause slip reactivation of pre-existing fault [18] when there is changes in hydraulic diffusivity [18,47,55], frictional strength and slip resistance. From our result, injecting at the middle and top of fault promotes such continuous fluid pressure elevation, which typically triggers slip event during the phase of hydraulic unloading (Fig. 4d). However, this aseismic event occurs at different timing for the two injector points, where Fig. 4b and c shows how the pore pressure build up rate affects the gradient of Coulomb stress ratio elevation. At the onset of shear failure, there is a sudden rise in pressure, and this corresponds to a sudden permeability increase, as observed for cases with mid and top injection. Generally, as observed in our results, induced seismicity is evident where the increase in pore pressure causes a reducing effect on the effective normal stress leading to the failure of a pre-existing fault [56].

Shear stress accumulation with injector at middle and bottom of fault maintain a seemingly uniform distribution from start of injection. While a sudden shear stress drop is registered for middle injection after injecting for 7.3 days, there is continuous shear build-up at bottom injection with no energy release. The shear stress for top injection condition is slightly less but injecting at this point results in the first noticeable shear failure with slip event occurring after 5 days of injection (Fig. 4e). Thus, with both top and mid injection, we observed a gradual shear rise after the first hydromechanical slip was recorded, however, this shear elevation produces a continuous permeability enhancement till injection stops.

Overall, result from the three cases showed permeability evolution which is pressure and stress dependent [57–59]. However, since the faults are of the same hydraulic properties and orientation, the variation in permeability enhancement is only considered as a function of the injection induced pressure emanating from the injector point.

During unloading, effective stress is lowest when the injector is at the top, concurrently, pressure is most elevated at this point. The stress state could improve or decline the stability condition around the fractured zone, which is revealed in our result, as sudden increase in effective stress produced fault slip in cases with top and mid injection. Hence, contour of fault permeability at the end of each injection is shown in Fig. 5a, b and c, where top injection (Fig. 5a) and mid injection (Fig. 5b) showed same permeability state, whereas, bottom injection shows low permeability enhancement (Fig. 5c).

Fig. 6 compares the slip distance profiles along the fault damage zone at different injection positions. This plot revealed that the injection induced instability potential of the fault is varied with the injection position, even though the injection rate remains constant. Obviously, this changing response is also responsible for the observed variations in

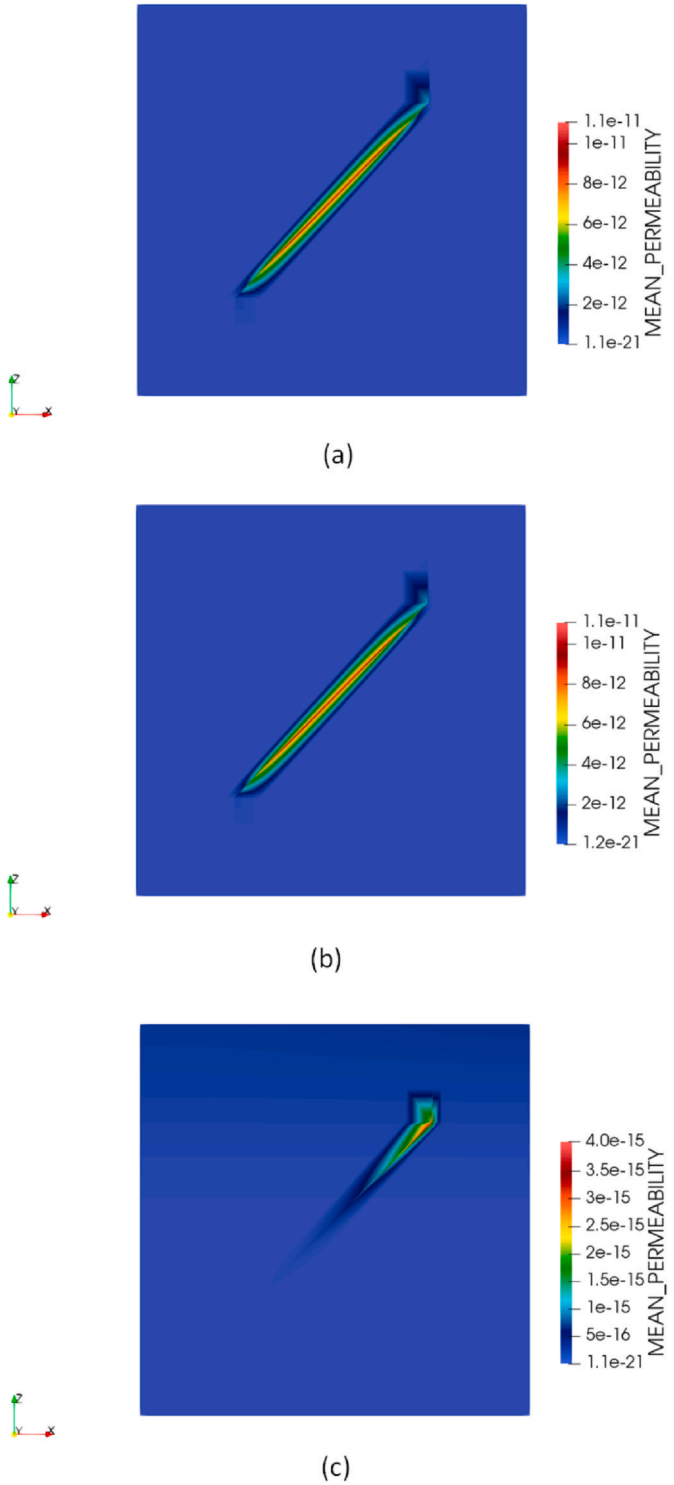

Fig. 5. Fault permeability at the end of Injection (a) Top injection (b) Mid injection (c) Bottom injection.

permeability evolution, because the most significant fault permeability enhancement is only observed with the onset of shear slip. Thus, slip rate and slip tendency of faults becomes a major influence on the permeability evolution. Our slip profile suggests that higher rate of fluid pressure diffusivity and increasing energy of diffusion have a dominant effect on the corresponding slip events. However, there is no pore pressure elevation and poroelastic stress changes which would promote fault reactivation at the bottom injector position. Consequently, there is no slip response in this injection case, and thus, permeability

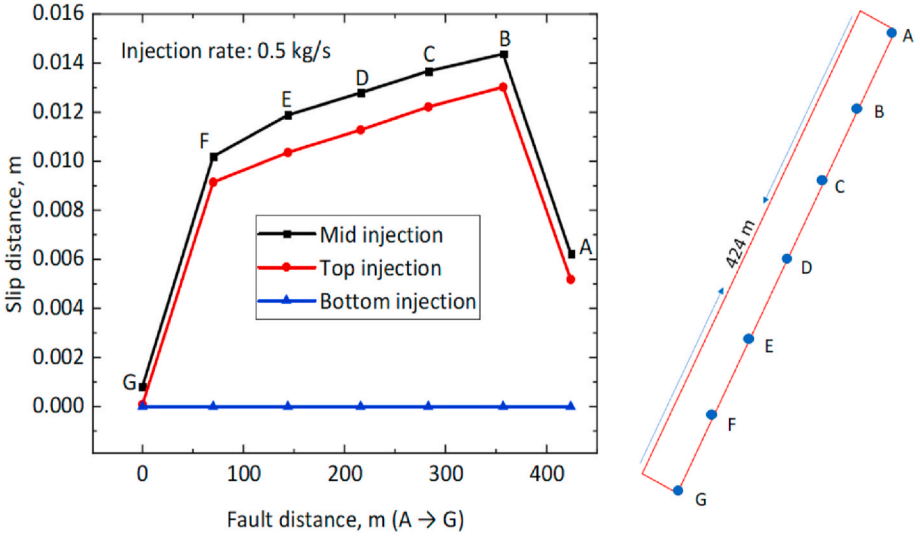

Fig. 6. Slip distance plot for the three injection positions at constant injection rate.

enhancement is insignificant.

Most often, fluid-driven aseismic slip can be developed further away from the zone immediately impacted by the injection [18], and this has implications on the entire fault plane reflecting different magnitudes of slip distances. The highest slip distance is located at the fault centre and decays as it approaches the lateral tips [16], thus, the lowest fault slip distance is at the two ends of the fault limbs as shown in Fig. 6. The slip distance when injector is placed at the mid of the fault is higher than the top position.

3.2. Influence of injection rate

Injection rate influences the velocity of fluid transmission, which determines the rate of pore pressure build-up within the fault damage zone [16]. It also reflects the timing of induced fault reactivation and the poroelastic response during fault slip. From our results, there is variation in permeability evolution and slip event as the injection rate changes.

We observed a systematic rise in permeability, and pore pressure build-up with stress relaxation at the start of injection (Fig. 7a). This is the unloading phase, with increasing propensity for failure [56]. Although there is no significant permeability difference in all the injection rates at this phase, the magnitude of effective stress reduction increases with lower injection rate (Fig. 7a, c and d).

The fault permeability in our model is both pressure and stress sensitive, the magnitude stress and pressure perturbation determined the extend of permeability enhancement directly. Permeability enhancement is limited under the sole pressurization effect Fig. 7a, c and d), as pressure elevation in injection rate 0.10 kg/s is unable to trigger shear failure. From this result, we deduced that the shear dilation and fault reactivation produced permeability enhancement which is more stress dependent. The evolution of pore pressure shows increasing pressure build-up as injection rate increases, conversely, stress accumulation during unloading reduces with increasing injection rate. However, with the increasing order of stress excitation as the rate reduces, the tendency of the fault to loading increases with increasing injection rate. Therefore, earlier onset of slip is observed with the highest injection rate, while 0.10 kg/s (the lowest rate) is not capable of inducing fault slip.

The variation in the loading rate showed that injection rate is firmly related to the increasing slip tendency, as Coulomb stress ratio plot revealed (Fig. 7b). With the injection rate set at 0.10 kg/s, there is no significant permeability enhancement because at this rate, the fault is not responsive to loading, thus, no shear enhanced permeability.

The sudden steep pressure rise observed with injection rate 0.20 kg/s and above showed that the shear dilation response of the fault due to reactivation causes stress excitation which promotes an increasing fault normal aperture [16]. This means, the evolving permeability changes the state of the fault aperture [50], depending on the magnitude of enhancement. This sudden steep pressure surge was caused by the compression of one side of the fault while the other side is dilated resulting in undrained pore pressure which is of opposite sign. The pore pressure is thus enhanced due to the created permeable channel. However, with dilation and increased volumetric strain, the already built pressure diffuses in order to equilibrate and maintain continuity of pore pressure level [51,52].

The shearing potential and frictional resistance of the fault with increasing rate are further explored by calculating their individual slip distance after slip event. The slip profile in Fig. 8 showed variation in fault slip distance after simulation was completed. As reported by Ref. [16], with increasing injection rate, the slip distance of fault increases correspondingly in space, and the highest slip distance is often located at the centre of the fault while it decays towards the lateral tips. A similar trend is observed with the slip profile in Fig. 8, where increasing injection rate elevates the slip distance of the fault. The high slip distance corresponding to high pore pressure (Fig. 7c) implies substantial fluid circulation in the evolving fault zone. Furthermore, because of fault dilation during slip, higher pore pressure drop promotes increasing fault strengthening [47,60], meanwhile, the slip becomes more stable when the pore pressure in the fault zone approaches hydrostatic level, because at this point, the conditions for fault stability would have been met [61].

As earlier reported, injection rate 0.10 kg/s did not record any slip event because the fluid pressure diffusivity at this rate could not trigger fault failure. Our slip profile indicates that a higher rate of fluid pressure diffusivity and increasing energy of diffusion have a dominant effect on the corresponding slip events. Therefore, at this injection rate, there is no pore pressure elevation and poroelastic stress changes to promote fault reactivation.

Fault permeability enhancement at the end of injection follows an increasing order of slip magnitudes as injection rate rises as shown in Figs. 7a and Fig. 9a–e.

4. Conclusions

In addition to the existing factors which support fault reactivation and permeability enhancement, this study has considered the contributions of injection location and injection rate on triggering fault

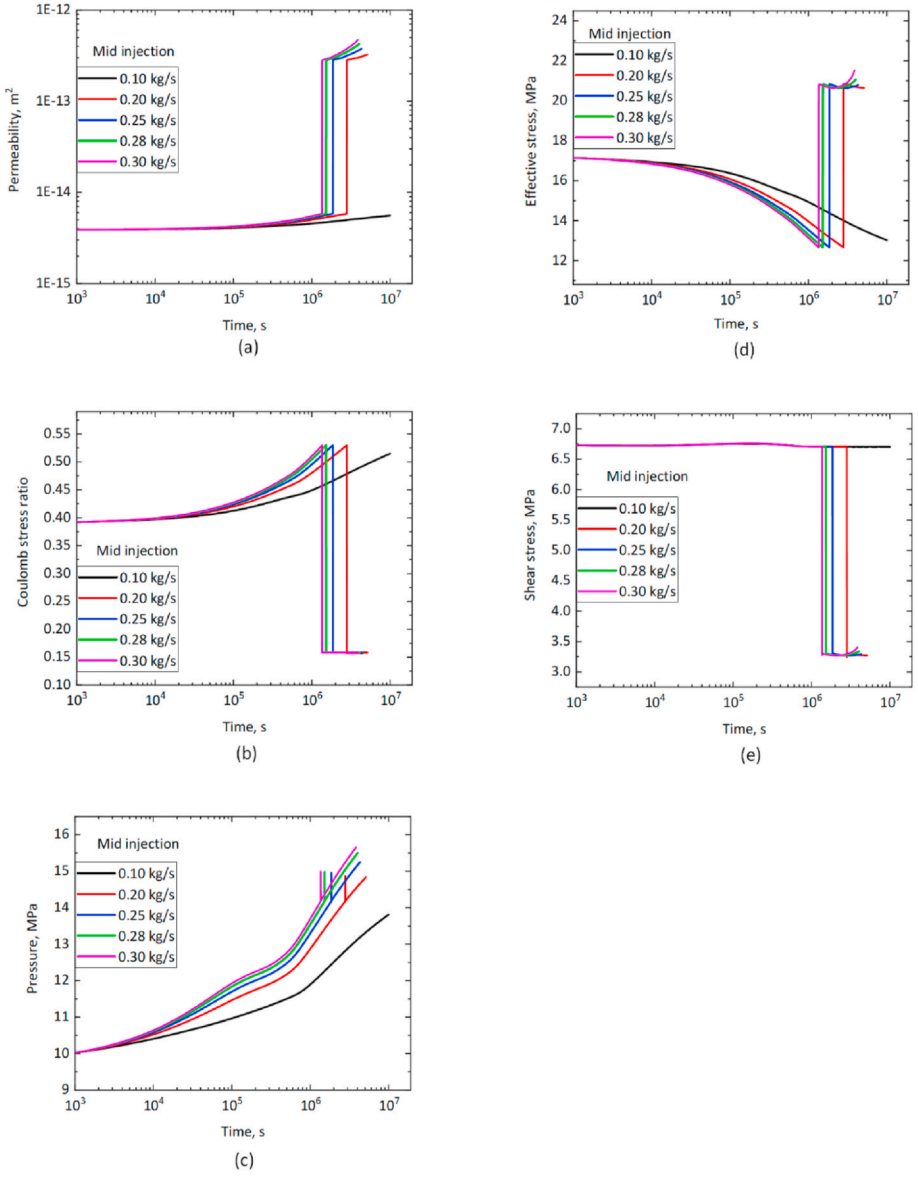

Fig. 7. (a) Evolution of fault permeability at changing injection rate (b) Evolution of Coulomb stress ratio showing variation in slip tendency with increasing injection rate (c) Evolution of pore pressure at various injection rate (d) Evolution effective stress with changing injection rate (e) Evolution of shear stress at various injection rate.

slip. The hydraulic diffusivity and permeability variations with changing injection scenarios were examined by comparing shear failure results, and thus presented variations in fracture response with injection well in three injection distinct locations. Overall, faults, which possess the same properties and architecture showed dissimilar response when injected from different points. The results therefore reveal that injection well placement along the fault significantly influenced the hydraulic diffusivity of the fluid pressure, which consequently determines the corresponding fault reactivation potential and permeability evolution. With injection rate at the base, there is declination in fluid volume distribution due to lower rate of diffusion, however, when the fluid pressure is released from the top, the hydraulic diffusivity is higher. This increasing diffusivity of fluid pressure has a first order effect on the pore pressure elevation and effective stress. As a result of the low pore pressure build-up at bottom injection, coupled with no stress change, this injection position is not capable of inducing shear failure, consequently, there is insignificant permeability enhancement, unlike the other two positions where shear failure induced the permeability increase. Although the resulting permeability at the end of simulation when the injection well is at the middle and at the top of fault are almost equal, the slip distance and induced seismicity in the later position is lower. Additionally, the criticality of the fault is influenced by the size of the slip zone, which is determined by the size of the fault surface area affected by high pore pressure. Nevertheless, we observed that the permeability evolution is affected by the maximum diffusion length and the size of the slip event.

Furthermore, we have presented simulation results of fault injection at increasing injection rate, to further understand the factors that promote fault reactivation potential and associated permeability evolution. Our results have showed that the dominant factor in shear failure is the stress change, and effective stress in the fault zone must respond to loading before any fracture failure can occur. Also, this study has established that there is a direct connection between permeability changes and effective stress changes in a fault zone, and that the degree of permeability increase in a fault zone where induced seismicity has been triggered is dependent on the rate of fluid pressure diffusivity and the accompanied seismic event.

Thus, since there is variation in lateral diffusivity of the fluid

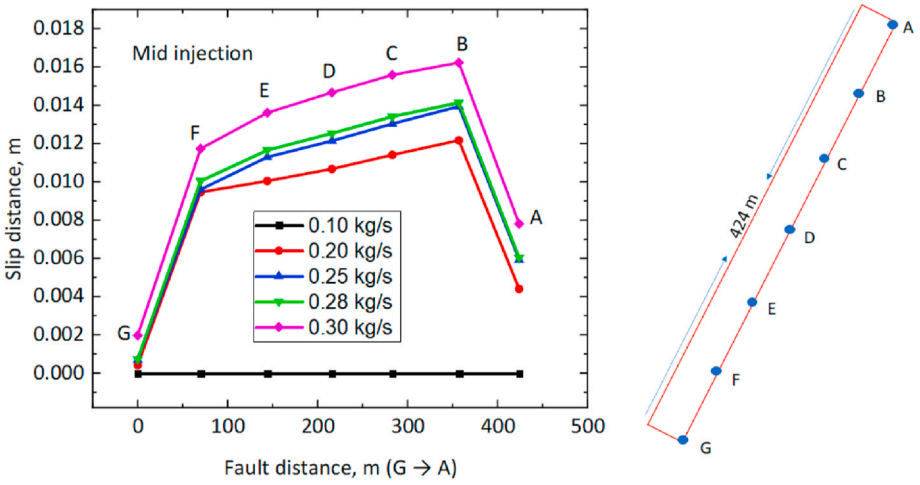

Fig. 8. Slip distance profile for the various injection rate under the same injection position from 0.1 kg/s to 0.3 kg/s showing increasing slip distance with increasing injection rate.

pressure emanating from changing injection positions and rate, it is essential to carefully choose the best position to situate an injection well, while also ensuring that the most suitable injection rate is adopted. This is to ensure desirable results, as the right choice would improve well productivity and ensure maximum control of the dynamic responses.

Acknowledgements

The authors wish to acknowledge Adekunle Ajasin University, for granting the lead author a study leave; the African Union for providing the financial support (scholarship) through the Pan African University; and the University of Aberdeen for providing the facilities and enabling environment for a successful research.

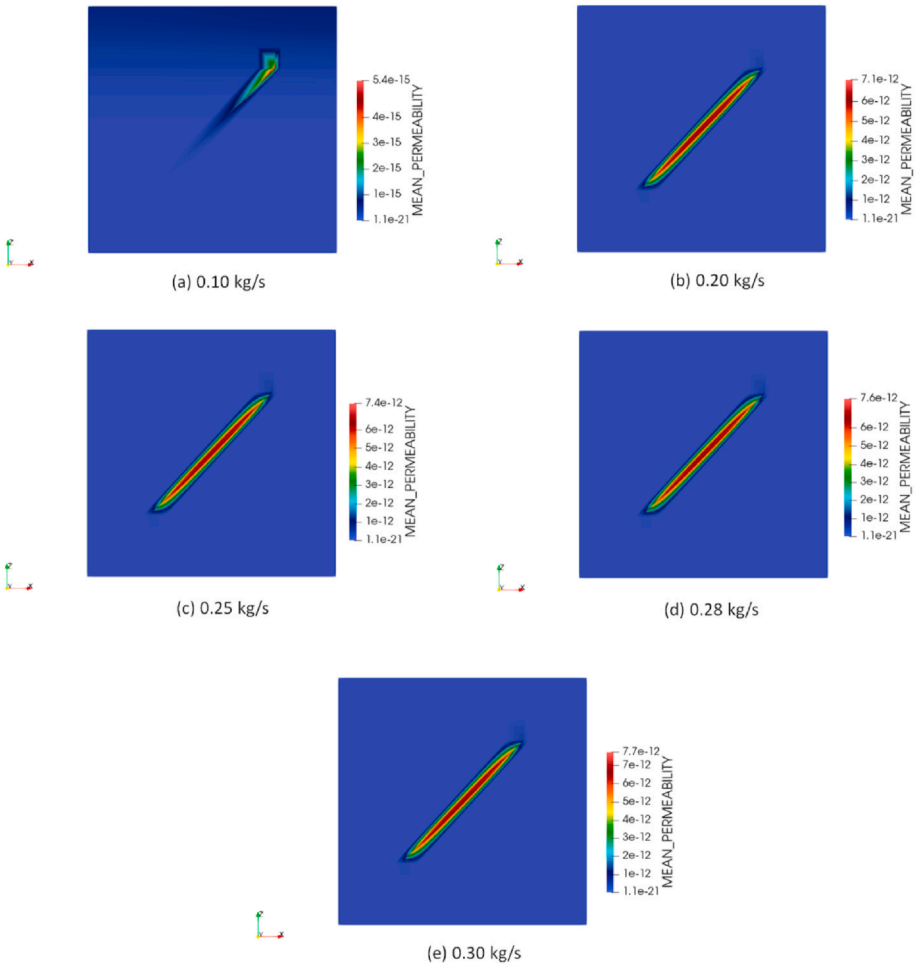

Fig. 9. Fault zone permeability at the end of injection with increasing magnitude from injection rate 0.1 kg/s to 0.6 kg/s.

References

[1] M.M. Hossain, M.K. Rahman, Numerical simulation of complex fracture growth during tight reservoir stimulation by hydraulic fracturing, J. Petrol. Sci. Eng. 60 (2) (2008) 86–104, https://doi.org/10.1016/j.petrol.2007.05.007.
[2] L.W. Bazan, B.R. Meyer, Fracture complexity: analysis methodology and signature pressure behavior of hydraulic fracture propagation from horizontal wellbores, SPE Asia Pacific Unconv. Res. Conf. Exhib. (2015), https://doi.org/10.2118/176919-ms.
[3] O. Kolawole, I. Ispas, Interaction between hydraulic fractures and natural fractures: current status and prospective directions, J. Petrol. Explor. Prod. Technol. (2019), https://doi.org/10.1007/s13202-019-00778-3.
[4] S. Rani, B.K. Prusty, S.K. Pal, Methane adsorption and pore characterization of Indian shale samples, J. Unconv. Oil Gas Resour. 11 (2015) 1–10.
[5] H. Wang, Numerical investigation of fracture spacing and sequencing effects on multiple hydraulic fracture interference and coalescence in brittle and ductile reservoir rocks, Eng. Fract. Mech. 157 (2016) 107–124.
[6] W.A.M. Wanniarachchi, R.P. Gamage, M.S.A. Perera, T.D. Rathnaweera, M. Gao, E. Padmanabhan, Investigation of depth and injection pressure effects on breakdown pressure and fracture permeability of shale reservoirs: an experimental study, Appl. Sci. 7 (2017) 664, https://doi.org/10.3390/app7070664 pg 1-25.
[7] V. Vilarrasa, R. Makhnenko, S. Gheibi, Geomechanical analysis of the influence of CO2 injection location on fault stability, J. Rock Mech. Geotech. Eng. 8 (2016) (2016) 805–818.
[8] C.T. Montgomery, M.B. Smith, Hydraulic Fracturing: History of an Unending Technology, JPT, 2006, pp. 26–41 December 2010.
[9] G.J. Massonat, E. Manisse, Evaluation of vertical permeability anisotropy in fractured reservoirs, Bull. Am. Assoc. Pet. Geol. 78 (1994) 1154.
[10] M. McClure, Characterizing hydraulic fracturing with a tendency for shear stimulation test, Presented at the SPE Annual Technical Conference and Exhibition held in New Orleans, Louisiana, USA, 30 September–2 October 2013 (1-17). SPE 166332-MS, 2013.
[11] Z. Ye, A. Ghassemi, Experimental study on injection-induced fracture propagation and coalescence for egs stimulation, PROCEEDINGS, 43rd Workshop on Geothermal Reservoir Engineering Stanford University, Stanford, California, February 12-14, 2018 SGP-TR-213. 1-9, 2018.
[12] A. Jacquey, M. Cacace, G. Blöcher, M. Scheck-Wenderoth, Numerical investigation of thermoelastic effects on fault slip tendency during injection and production of geothermal fluids, Energy Procedia 76 (2015) 311–320, https://doi.org/10.1016/j.egypro.2015.07.868.
[13] J.E. Streit, R.R. Hillis, Estimating fault stability and sustainable fluid pressures for underground storage of CO2 in porous rock, Energy 29 (2004) 1445–1456.
[14] Q. Gan, D. Elsworth, J.S. Alpern, C. Marone, P. Connolly, Breakdown pressures due to infiltration and exclusion in finite length boreholes, J. Petrol. Sci. Eng. 127 (2015) 329–337, https://doi.org/10.1016/j.petrol.2015.01.011.
[15] Q. Gan, D. Elsworth, Production optimization in fractured geothermal reservoirs by coupled discrete fracture network modelling, Geothermics 62 (2016) 131–142, https://doi.org/10.1016/j.geothermics.2016.04.009.
[16] Q. Gan, Q. Lei, Induced fault reactivation by thermal perturbation in enhanced geothermal systems, Geothermics 86 (2020) 101814, , https://doi.org/10.1016/j.geothermics.2020.101814 1-12.
[17] D.S. Eyinla, M.A. Oladunjoye, Empirical analysis for the characterization of geomechanical strength and pressure regime: implications on hydraulic fracturing stimulation, Petroleum (2018), https://doi.org/10.1016/j.petlm.2018.05.002 (2018).
[18] F. Cappa, Y. Guglielmi, C. Nussbaum, J. Birkholzer, On the relationship between fault permeability increases, induced stress perturbation, and the growth of aseismic slip during fluid injection, Geophys. Res. Lett. 45 (2018), https://doi.org/10.1029/2018GL080233.
[19] J.B. Altmann, T.M. Müller, B.I. Müller, M.R. Tingay, O. Heidbach, Poroelastic contribution to the reservoir stress path, Int. J. Rock Mech. Min. Sci. 47 (2010) (2010) 1104–1113.
[20] S. Kim, S.A. Hosseini, Geological CO2 storage: incorporation of pore-pressure/stress coupling and thermal effects to determine maximum sustainable pressure limit, Energy Procedia 63 (2014) 3339–3346, https://doi.org/10.1016/j.egypro.2014.11.362.
[21] M.L. Doan, E.E. Brodsky, Y. Kano, K.F. Ma, In situ measurement of the hydraulic diffusivity of the active Chelungpu Fault, Taiwan, Geophys. Res. Lett. 33 (2006) L16317, , https://doi.org/10.1029/2006GL026889.
[22] A. Nur, J. Booker, Aftershocks induced by pore fluid flow, Science 175 (1972) 885–887.
[23] F. Cappa, J. Rutqvist, Modeling of coupled deformation and permeability evolution during fault reactivation induced by deep underground injection of CO2, Int. J. Greenhouse Gas Contr. 5 (2011) (2011) 336–346, https://doi.org/10.1016/j.ijggc.2010.08.005.
[24] Q. Li, H. Xing, I. Liu, X. Liu, A review on hydraulic fracturing of unconventional reservoir, Petroleum 1 (2015) (2015) 8–15, https://doi.org/10.1016/j.petlm.2015.03.008.
[25] J.H. Dieterich, Earthquake nucleation on faults with rate-and state-dependent strength, Tectonophysics 211 (1–4) (1992) 115–134, https://doi.org/10.1016/0040-1951(92)90055-b.
[26] C. Marone, The effect of loading rate on static friction and the rate of fault healing during the earthquake cycle, Nature 391 (6662) (1998) 69–72, https://doi.org/10.1038/34157.
[27] S.M. Hsiung, A.H. Chowdhury, M.S. Nataraja, Numerical simulation of thermal-mechanical processes observed at the drift-scale heater test at yucca mountain, Nevada, USA, Int. J. Rock Mech. Min. Sci. 42 (2005) 652–666.
[28] M. Bai, D. Elsworth, Modeling of subsidence and strain-dependent hydraulic conductivity for intact and fractured porous media, Rock Mech. Rock Eng. 27 (1994) 209–250.
[29] J.W. Rudnicki, Fluid mass sources and point forces in linear elastic diffusive solids, Mech. Mater. 5 (1986) 383–393.
[30] F. Cappa, Y. Guglielmi, J. Virieux, Stress and fluid transfer in a fault zone due to overpressures in the seismogenic crust, Geophys. Res. Lett. 34 (2007) L05301, , https://doi.org/10.1029/2006GL028980.
[31] J.E. Warren, P.J. Root, The behavior of naturally fractured reservoirs, Old Spe J 3 (3) (1963) 245–255.
[32] N. Barton, V. Choubey, The shear strength of rock joints in theory and practice, Rock Mech. 10 (1–2) (1977) 1–54, https://doi.org/10.1007/bf01261801.
[33] S.C. Bandis, A.C. Lumsden, N.R. Barton, Fundamentals of rock joint deformation, Int. J. Rock Mech. Min. Sci. Geomech. Abstr. 20 (6) (1983) 249–268, https://doi.org/10.1016/0148-9062(83)90595-8.
[34] Q. Gan, D. Elsworth, Analysis of fluid injection-induced fault reactivation and seismic slip in geothermal reservoirs, J. Geophys. Res. Solid Earth 119 (2014) 3340–3353, https://doi.org/10.1002/2013JB010679.
[35] J. Rutqvist, O. Stephansson, The role of hydromechanical coupling in fractured rock engineering, Hydrogeol. J. 11 (1) (2003) 7–40, https://doi.org/10.1007/s10040-002-0241-5.
[36] D. Wiprut, M.D. Zoback, Fault reactivation and fluid flow along a previously dormant normal fault in the northern North Sea, Geology 2000 28 (2000) 595–598.
[37] M.J. Ikari, A.R. Niemeijer, C. Marone, Experimental investigation of incipient shear failure in foliated rock, J. Struct. Geol. 77 (2015) 82–91, https://doi.org/10.1016/j.jsg.2015.05.012.
[38] X. Wei, Q. Li, X. Li, Z. Niu, X. Liu, L. Liang, Effects of different penetration patterns on a fault during underground fluid injection, Geofluids (2019) 1–15, https://doi.org/10.1155/2019/2027510 2019, Article ID 2027510, 15 pages.
[39] K. Terzaghi, Die Berechnung der Durchlässigkeitsziffer des Tones aus dem Verlauf der hydrodynamischen Spannungserscheinungen (In German.), in: Sitz Akad, Wissen Wien (Eds.), Math-Naturw. Kl. Abt. IIa. vol. 132, 1923, pp. 105–124.
[40] M. Biot, General theory of three-dimensional consolidation, J. Appl. Phys. 12 (2) (1941) 155–164.
[41] J. Byerlee, Friction of rocks, Pure and Applied Geophysics PAGEOPH 116 (4–5) (1978) 615–626, https://doi.org/10.1007/bf00876528.
[42] J.C. Jaeger, N.G.W. Cook, Fundamentals of Rock Mechanics, third ed., Chapman and Hall, London, United Kingdom, 1979 593.
[43] J. Taron, D. Elsworth, K.B. Min, Numerical simulation of thermal–hydrologic-mechanical–chemical processes in deformable, fractured porous media, Int. J. Rock Mech. Min. Sci. 46 (5) (2009) 842–854, https://doi.org/10.1016/j.ijrmms.2009.01.008.
[44] Itasca Consulting Group, Inc, Fast Lagrangian Analysis of Continua in 3-dimensions, version 4.0 Minneapolis. Itasca Consulting Group, Minnesota, 2009 438.
[45] J. Rutqvist, Y.-S. Wu, C.-F. Tsang, G. Bodvarsson, A modeling approach for analysis of coupled multiphase fluid flow, heat transfer, and deformation in fractured porous rock, Int. J. Rock Mech. Min. Sci. 39 (2002) 429–442.
[46] M. Kinoshita, K. Shiraishi, E. Demetriou, Y. Hashimoto, W. Lin, Geometrical dependence on the stress and slip tendency acting on the subduction megathrust of the Nankai seismogenic zone off Kumano, Prog Earth Planet Sci 6 (2019) 7, https://doi.org/10.1186/s40645-018-0253-y.
[47] Y. Guglielmi, F. Cappa, J.P. Avouac, P. Henry, D. Elsworth, Seismicity triggered by fluid injections induced aseismic slip, Science 348 (6240) (2015) 1224–1226, https://doi.org/10.1126/science.aab0476.
[48] A. Zang, V. Oye, P. Jousset, N. Deichmann, R. Gritto, A. McGarr, E. Majer, D. Bruhn, Analysis of induced seismicity in geothermal reservoirs—an overview, Geothermics 52 (2014) 6–21, https://doi.org/10.1016/j.geothermics.2014.06.005.
[49] F. Wang, Z. Mi, Z. Sun, X. Li, T. Lan, Y. Yuan, T. Xu, Experimental study on the effects of stress variations on the permeability of feldspar-quartz sandstone, Hindawi Geofluids 2017 (2017), https://doi.org/10.1155/2017/8354524 Article ID 8354524, 15 pages.
[50] M. Manga, I. Beresnev, E.E. Brodsky, J.E. Elkhoury, D. Elsworth, S.E. Ingebritsen, D.C. Mays, C.Y. Wang, Changes in permeability caused by transient stresses: field observations, experiments, and mechanisms, Rev. Geophys. 50 (2012) RG2004, , https://doi.org/10.1029/2011RG000382.
[51] E.M. Dunham, J.R. Rice, Poroelastic Bimaterial Effects in Rupture Dynamics, AGU Fall Meeting Abstracts, 2006 December 2006.
[52] N.R. Iverson, T.S. Hooyer, U.H. Fischer, D. Cohen, P.L. Moore, M. Jackson, G. Lappegard, J. Kohler, Soft-bed experiments beneath Engabreen, Norway: regulation infiltration, basal slip and bed deformation, J. Glaciol. 53 (182) (2007) 323–340.
[53] M. Schoenball, T. Müller, B. Müller, O. Heidbach, Fluid-induced microseismicity in pre-stressed rock masses, Geophys. J. Int. 180 (2010) (2010) 813–819.
[54] V. Vilarrasa, J. Carrera, S. Olivella, Hydromechanical characterization of CO2 injection sites, Int. J. Greenhouse Gas Contr. 19 (2013) (2013) 665–677.
[55] M.M. Scuderi, C. Collettini, The role of fluid pressure in induced vs. triggered seismicity: insights from rock deformation experiments on carbonates, Nat. Sci. Rep. 6 (1) (2016) 24852, https://doi.org/10.1038/srep24852.
[56] M.K. Hubbert, W. Rubey, Role of fluid pressure in mechanics of overthrust faulting, Geol. Soc. Am. Bull. 70 (1959) 115–205, https://doi.org/10.1130/0016-7606(1959)70[115:ROFPIM]2.0.CO;2.
[57] R.D. Barree, V.L. Barree, D. Craig, Holistic fracture diagnostics: consistent interpretation of prefrac injection tests using multiple analysis methods, SPE Prod. Oper. 24 (3) (2009) 396–406, https://doi.org/10.2118/107877-PA.

[58] Y. Cho, O.G. Apaydin, E. Ozkan, Pressure-Dependent Natural-Fracture Permeability in Shale and its Effect on Shale-Gas Well Production, SPE Reservoir Evaluation & Engineering, 2013 Pg 216-228.
[59] H.Y Wang, M.M. Sharma, Determine in-situ stress and characterize complex fractures in naturally fractured reservoirs from diagnostic fracture injection tests, Rock Mech. Rock Eng. 52 (12) (2019) 5025–5045, https://doi.org/10.1007/s00603-019-01793-w.
[60] P. Segall, J. Rice, Dilatancy, compaction, and slip instability of a fluid-infiltrated fault, J. Geophys. Res. 100 (B11) (1995) 22,155–22,171, https://doi.org/10.1029/95JB02403 (Wiley Online Library ADS Web of Science®Google Scholar).
[61] C.H. Scholz, Earthquakes and friction laws, Nature 391 (6662) (1998) 37–42, https://doi.org/10.1038/34097.